Showcasing collaborative research from Illinois Institute of Technology and University of Texas, USA and Bhabha Atomic Research Centre, India

Single red emission from upconverting $ZnGa_2O_4$:Yb,Er nanoparticles co-doped by Cr^{3+}

Bright singular red emission from $ZnGa_2O_4$:Yb,Er upconversion nanoparticles after Cr^{3+} co-doping and annealing for efficient diffusion and even distribution of dopant ions into the host lattice and the reduction of surface defects will have great application prospects in biological imaging, security applications and display devices.

As featured in:
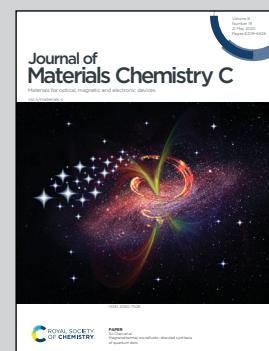
ROYAL SOCIETY OF CHEMISTRY

rsc.li/materials-c

Registered charity number: 207890

PAPER

Check for updates

Single red emission from upconverting ZnGa$_2$O$_4$:Yb,Er nanoparticles co-doped by Cr^{3+}†

Bhupendra B. Srivastava,[a] Santosh K. Gupta [ID][b] and Yuanbing Mao [ID]*[c]

Near infrared (NIR) to visible upconversion has been the focus in the optical research community considering bioimaging applications mainly because NIR excitation has a deep penetration depth, low autofluorescence and high damage threshold to tissues. The Yb^{3+}–Er^{3+} sensitizer–activator combination has been the preferred choice among upconversion nanophosphors (UCNPs) since it efficiently upconverts 980 nm light to green (550 nm) and red (660 nm) emissions. However, the green emission from this Yb/Er combination is undesirable because its escape from tissues is extremely difficult, and thus may cause damage to cell/tissues, which decreases the overall bioimaging sensitivity. Also, realizing manganese-free single emission in Yb–Er-based UCNPs is of great relevance since the multiple oxidation states of manganese can sometimes disturb the sensitizer-to-dopant energy transfer (ET) kinetics. Moreover, Cr^{3+} has a higher absorption coefficient for green color compared to manganese ions. Therefore, in this study, we first synthesized ZnGa$_2$O$_4$:Yb^{3+},Er^{3+},Cr^{3+} (ZGO-YEC) nanoparticles (NPs) *via* a hydrothermal method at 120 °C with judicious Cr^{3+} co-doping. Through further high temperature annealing, wherein a large fraction of doping ions is included inside the host lattice, these ZGO-YEC NPs emit a bright single red emission under 980 nm excitation. This process is facilitated by the absorption of green emission *via* the Er^{3+} → Cr^{3+} ET, followed by back ET to the ^{4}F$_{9/2}$ level of Er^{3+}. They also directly emit NIR emission under 254 nm excitation. This luminescing ability can only be deciphered when dual NIR and UV excitations exist simultaneously, which makes illegal imitation very difficult to implement, thus improving the level of anticounterfeiting. This work provides an effective approach to obtain manganese-free UCNPs with bright red UC luminescence for the first time, which may be suitable for biological imaging, security applications, and optical probes for magnetic resonance imaging.

1. Introduction

Light plays an important role in human life for inducing many critical biological phenomena.[1,2] Its high degree of spatial and temporal resolution and the ease of tuning its wavelength and intensity make it an ideal stimuli for *in situ* chemical and biological manipulations.[3] Among various light-emitting materials, upconversion (UC) nanoparticles (NPs), which convert low energy photons into high energy photons, have been attracting increasing attention in the scientific community because of their applications in various areas of science and technology.[4] UCNPs have been exploited in several applications, which are directly associated with daily life such as optoelectronic devices,[5] anticounterfeiting,[6]

photodynamic therapy,[7] bioimaging,[3] renewable energy,[8] and thermochromic phosphors for switching devices.[9]

The design of high quality and efficient UCNPs requires judicious choice of host lattices and dopant ions. In most cases, it has been found that lanthanide ions are ideal dopants. Because of their unique photophysical properties such as high color purity, narrow emission profile, long excited state lifetime owing to forbidden f–f transition, and negligible influence of ligand/crystal field on the ground state and excited state wave functions, they are the most extensively used dopants in designing luminescent materials.[10–12] Thus, we proposed the uses of ZnGa$_2$O$_4$ (ZGO) as one of the most promising UC host materials because it exhibits all the desirable properties of a host, such as high chemical/thermal stability, wide band gap, ease of synthesis, biocompatibility, and non-toxicity. Previously, our group reported bright red persistence luminescence from sub-10 nm ZnGa$_2$O$_4$:Cr^{3+} nanocrystals.[13] In this study, considering the dopant (activator) ions, we propose the use of a combination of Yb^{3+} and Er^{3+}, which are known to display green (550 nm) and red emission bands (660 nm).[4] The red and near infrared (NIR) spectral regions in the range of 600–700 nm and 700–1100 nm, respectively,

^{a} *Department of Chemistry, University of Texas Rio Grande Valley,*
1201 West University Drive, Edinburg, Texas 78539, USA
^{b} *Radiochemistry Division, Bhabha Atomic Research Centre, Trombay,*
Mumbai 400085, India
^{c} *Department of Chemistry, Illinois Institute of Technology, 3105 South Dearborn Street,*
Chicago, IL 60616, USA. E-mail: ymao17@iit.edu; Tel: +1-312-567-3815
† Electronic supplementary information (ESI) available. See DOI: 10.1039/d0tc00411a

6370 | *J. Mater. Chem. C*, 2020, **8**, 6370–6379

This journal is © The Royal Society of Chemistry 2020

are considered the most ideal optical range for biological tissues owing to their low absorption in tissues and large penetration range.[14] Green emission from the Yb/Er combination is undesirable because its escape from tissues is extremely difficult, which decreases the overall bioimaging sensitivity. Therefore, the green/red emission output should be tuned in such a way that green emission is minimized, while red emission is maximized for *in vivo* imaging applications. However, exploring this ideal scenario using Yb^{3+}/Er^{3+}-based UCNPs is extremely difficult and challenging, while it is essential to achieve intense single red emission with negligible green band for high-quality deep tissue imaging using UCNPs.[15] As a result, bringing both excitation and emission maxima in the optical range of biological tissues are quite challenging for deep tissue applications of fluorescent labels.

In most cases, the red/green emission ratio of the Er^{3+}/Yb^{3+} combination is tuned by altering the sensitizer to activator ratio or optimizing the synthetic conditions, while completely eliminating the green emission is very difficult.[16–18] There have been a few reports where researchers tuned Er^{3+}/Yb^{3+}-based UC phosphors to generate a single red emission. Xie *et al.* reported a single red emission in $MnF_2:Er^{3+}/Yb^{3+}$ NPs induced by Mn^{2+} to Er^{3+} energy transfer (ET), but there are numerous issues associated with fluorine-based hosts owing to the high toxicity of the fluorine.[19] Also, the synthesis was complicated since size control was achieved by adding additional polyethylene amine. Bai *et al.* also reported singular red emission in both MnF_2 and $NaMnF_3$ induced by host Mn^{2+} to Er^{3+} ET with substantial green peak still present.[20,21] Wang *et al.* reported a novel oil-based procedure for the synthesis of lanthanide-doped $KMnF_3$ nanocrystals with only single-band UC emissions from Er^{3+}, Ho^{3+}, and Tm^{3+} dopants, respectively.[22] Tian *et al.* produced pure red emission from $NaYF_4:Er^{3+}/Yb^{3+}$ NPs by co-doping with Mn^{2+}.[15] Lin *et al.* achieved the same in $NaLuF_4:Er^{3+}/Yb^{3+}$ NPs by pH adjustment.[23] However, the latter two reports had issues with the involvement of fluorine and complex synthetic procedures.

Manganese photochemistry is complex owing to its several oxidation states compared to chromium ions, which have oxidation numbers of 0, +2, +3 and +6. In contrast, because it possesses one extra electron, manganese shows more oxidation states: 0, +2, +3, +4, +6 and +7. Moreover, interference between the red emission of Mn^{2+} in a strong O_h field and Er^{3+} red emission occurs, whereas Cr^{3+} emits in the near IR region around 700 nm. There are a few reports wherein the Cr^{3+} ion was co-doped with the Yb^{3+}/Er^{3+} combination, but no singular red emission has been reported from these combinations. Tuomisto *et al.* reported the observation of UC from $NaYF_4:Yb^{3+}:Er^{3+}$ co-doped with Cr^{3+} at a low power density and improved overall luminescence intensity.[24] They also found that Mn^{2+} co-doping weakened the UC intensity of $NaYF_4:Yb^{3+}:Er^{3+}$. Mikalauskaite *et al.* investigated the effect of Cr^{3+} concentration on the red/green ratio of $NaGdF_4:Yb^{3+}:Er^{3+}$, but could not achieve singular red emission.[25] Ye *et al.* demonstrated that the UC of $La_3Ga_5GeO_{14}:Yb^{3+},Er^{3+}$ was sensitized by a low concentration of Cr^{3+} doping and the ET proceeded *via* the Yb^{3+} bridge.[26] Huy *et al.* improved the UC intensity of β-$NaLuGdF_4:Yb,Er$ NPs by 20 times by Cr^{3+} co-doping with induced cubic-hexagonal phase transition.[27]

There are also a few other reports of chromium-sensitized UC in organometallic and d–f bimetallic complexes.[28,29]

Furthermore, there are some reports on the UC luminescence of ZGO with Er^{3+}/Yb^{3+} co-doping. Liu *et al.*[30] and Cheng *et al.*[31] explored the UC luminescence of $ZGO:Yb^{3+},Tm^{3+},Er^{3+}$ and ZGO: Yb^{3+},Er^{3+} (ZGO-YE) microcrystals synthesized *via* the solid-state method, respectively. Cheng's group also attempted to enhance the UC efficiency of ZGO-YE by Al^{3+} co-doping. However, all the above studies focused on bulk crystals with an interference of blue/green emission with red emission of Er^{3+}/Yb^{3+}, and the reduced efficacy is undesirable for several singular emission applications, particularly in bioimaging. Clinical procedures require injected bioimaging agents to be cleared from the human body as quickly as possible. As the main clearance route for bioimaging agents, the renal mode requires the particle size (including surface modifiers) to be smaller than 10 nm, and thus bulk materials are not suitable for biological applications.[32] Therefore, there is an urgent need for singular emission UCNPs for biological applications and the development of new or modified synthetic strategies to prepare sub-10 nm UCNPs is of crucial importance. Moreover, we can appropriately control the phase, size, shape and doping concentration of UCNPs at the nanometer scale.[33]

In this work, we hydrothermally synthesized $ZGO:Yb^{3+}$, Er^{3+},Cr^{3+} (ZGO-YEC) NPs and explored their photophysical properties. We produced singular red emission from these ZGO-YCE NPs induced by the absorption of green emission *via* $Er^{3+} \rightarrow Cr^{3+}$ ET followed by back ET to the $^4F_{9/2}$ level of Er^{3+} after further annealing treatment of the as-prepared ZGO-YEC NPs. This work opens a new gateway for the design of sub-10 nm doped ZGO NPs with optimum UC performances and singular red emission, and also provides a new strategy for the effective triple doping of Yb^{3+}, Er^{3+}, and Cr^{3+} ions into a single host.

2. Experimental

2.1 Materials

Zinc nitrate hexahydrate $(Zn(NO_3)_2 \cdot 6H_2O, 98\%)$, gallium nitrate hydrate $(Ga(NO_3)_3 \cdot xH_2O, 99.9\%)$, chromium nitrate nonahydrate $(Cr(NO_3)_3 \cdot 9H_2O, 99\%)$, erbium(III) nitrate pentahydrate $(Er(NO_3)_3 \cdot 5H_2O, 99.9\%)$, ytterbium(III) nitrate pentahydrate $(Yb(NO_3)_3 \cdot 5H_2O, 99.9\%)$, ammonium hydroxide solution $(28.0–30.0\% NH_3$ basis), and urea $(NH_2CONH_2, 99.0–100.5\%)$ were purchased from Sigma Aldrich. Ethyl alcohol (technical grade) were purchased from Fisher Scientific. All the chemicals were analytical grade reagents and used directly without further purification.

2.2 Synthesis

$Zn(NO_3)_2$, $Ga(NO_3)_3$, $Y(NO_3)_3$, $Er(NO_3)_3$ and $Cr(NO_3)_3$ with the required concentrations were dissolved in 30 mL water. Ammonia solution was added to the solution to adjust its pH to the desired value and stirred for 30 min. Subsequently, the solution was transferred to a 45 mL Teflon-lined stainless-steel autoclave. The sealed autoclave was heated at 120 °C for 10 h. Afterward, the system was left to cool to room temperature and the resulting NPs

This journal is © The Royal Society of Chemistry 2020

J. Mater. Chem. C, 2020, **8**, 6370–6379 | **6371**

were precipitated from the synthesis solution with an excess volume of ethanol–water mixture. The purified products were separated by centrifugation and subsequently washed with an ethanol–water mixture two more times. The washed precipitates were dried at 110 °C in a drying oven overnight to obtain the ZGO-YEC NP powder.

2.3 Instrumentation

Powder X-ray diffraction (XRD) patterns of the ZGO-YEC NPs were measured with a Bruker D8 ADVANCE X-ray diffractometer with Cu K$_{\alpha 1}$ radiation ($\lambda = 0.15406$ nm). XRD data was collected utilizing the scanning mode in the 2θ range of 20° to 80°

with a scanning step size of 0.04° and a scanning rate of 2.0° min^{-1}. Transmission electron microscopy (TEM) and high-resolution TEM (HRTEM) images were recorded using a Hitachi HF 3300 TEM/STEM system. X-ray photoelectron spectroscopy (XPS) spectra were measured using a Thermo Scientific K-Alpha XPS with an 180° double-focusing hemispherical analyzer and 128 channel detector. PL emission and excitation spectra were recorded using an Edinburgh Instrument FLS 980 fluorimeter system having a steady state xenon lamp source. UC luminescence measurements were carried out on the same PL system, which was equipped with an MDL-III-980-2W Class IV laser.
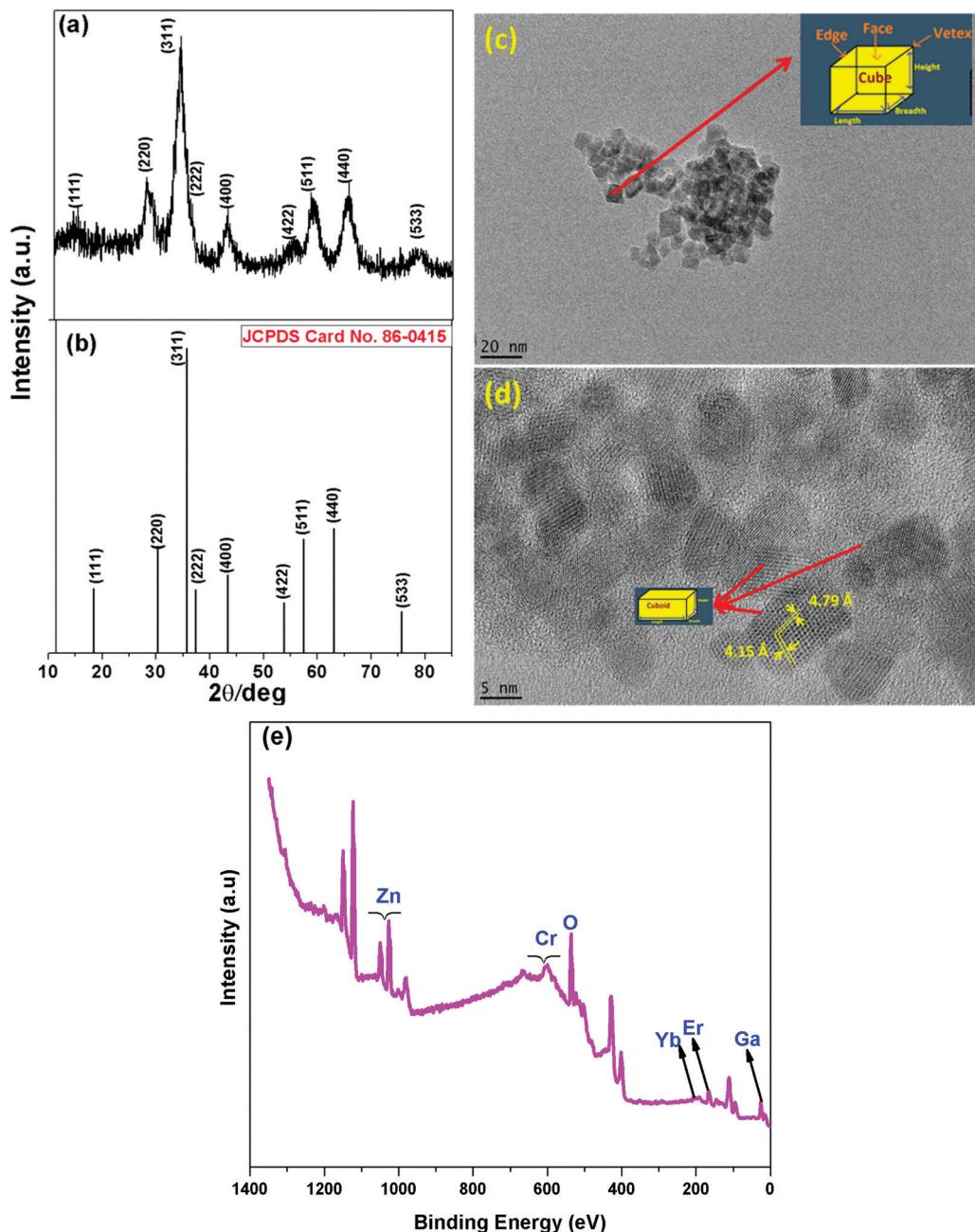

Fig. 1 (a) XRD pattern, (b) standard stick pattern of ZnGa$_2$O$_4$ corresponding to JCPDS file No. 86-0415, (c) TEM image, (d) HRTEM image, and (e) XPS survey scan of the as-prepared ZGO-YEC NPs.

6372 | *J. Mater. Chem. C*, 2020, **8**, 6370–6379

This journal is © The Royal Society of Chemistry 2020

3. Results and discussion

3.1 Phase purity, size and morphology: XRD, XPS and TEM

The XRD pattern of the as-prepared ZGO-YCE NPs at 120 °C (ZGO-YCE-AP) (Fig. 1a) confirms its pure and single crystalline phase of cubic spinel-structured $ZnGa_2O_4$. The pattern matches completely with the standard pattern of $ZnGa_2O_4$, corresponding to JCPDS Card No. 86-0415. All the reflection peaks match with that of pristine ZGO. The crystallite size of the ZGO-YCE-AP NPs is ~3 nm, as calculated using the Scherer equation. The representative TEM and HRTEM images of the ZGO-YCE-AP NPs (Fig. 1c and d, respectively) show the formation of small particles with well-defined boundaries and clear facets, e.g. nanocubes, in the range of several nanometers. The measured d-spacings of 4.79 and 4.15 Å originate from the (111) and (002) planes of cubic $ZnGa_2O_4$, respectively. The XPS survey scan of the ZGO-YCE-AP NPs (Fig. 1e) confirmed the presence of Zn, Ga, O, Er, Yb and Cr elements.

The detailed XPS spectra of the ZGO-YEC-AP NPs are shown as Fig. 2a–f, corresponding to Zn 2p, Ga 3d, O 1s, Er 4d, Yb 3d and Cr 2p orbitals, respectively. Moreover, the presence of the activator Er^{3+} ions, sensitizer Yb^{3+} ions, and co-dopant Cr^{3+} ions is clearly confirmed by the XPS spectra shown in Fig. 2d–f, respectively.

After thermal annealing up to 800 °C, the XRD patterns (Fig. 3a) demonstrated that all the thermally treated samples were still pure as the $ZnGa_2O_4$ host (JCPDS Card No. 38-1240). Moreover, the crystalline size of the ZGO-YCE NPs did not grow to a large extent. The calculated crystalline size of the samples is in the range of around 3–10 nm. The thermally treated samples were designated as ZGO-YCE-annealing temperature.

The representative TEM image (Fig. 3b) of the ZGO-YCE-700 NPs shows that there was not much increase in the size of the NPs. Based on the size distribution plot (inset of Fig. 3b), the average size of the ZGO-YCE-700 NPs is ~7 nm.

3.2 Photoluminescence spectroscopy

3.2.1 Dual UC and DC emission from the ZGO-YEC NPs: role of chromium ion.
The UC emission spectra of the ZGO-YEC-AP and ZGO-YEC-700 NPs under 980 nm laser excitation (Fig. 4a) exclusively consist of three main peaks located at around 525 nm, 550 nm, and 660 nm, which are attributed to the inter-configurational f–f transitions of the trivalent Er^{3+} ions. The dual bands of 525 nm and 550 nm located in the green region (G-bands) of the electromagnetic spectrum are due to the $^2H_{11/2} \rightarrow {}^4I_{15/2}$ and $^4S_{3/2} \rightarrow {}^4I_{15/2}$ transitions of the Er^{3+} ions. The band at 660 nm located in the red region (R-band) is ascribed to the $^4F_{9/2} \rightarrow {}^4I_{15/2}$ transition of the Er^{3+} ions. Most significantly, there was a drastic improvement in the UC intensity of the R-band from the ZGO-YEC-700 NPs compared to the ZGO-YEC-AP NPs together with a distinct change in their spectral profiles. For the ZGO-YEC-AP NPs, the integral intensity of the G- and R-bands is in a similar order. For the ZGO-YEC-700 NPs, the R-band completely dominates compared to the G-bands. Specifically, a singular red emission could be observed with almost compete quenching of the green emission.

The ZGO-YEC samples also show downconversion (DC) emission under UV excitation at 254 nm (Fig. 4b). The band at around 700 nm with a quantum yield of 10.31% with several fine spectral features is attributed to the $^2E \rightarrow {}^4A_2$ transition of the trivalent Cr^{3+} ions. These peaks are attributed to the distribution of
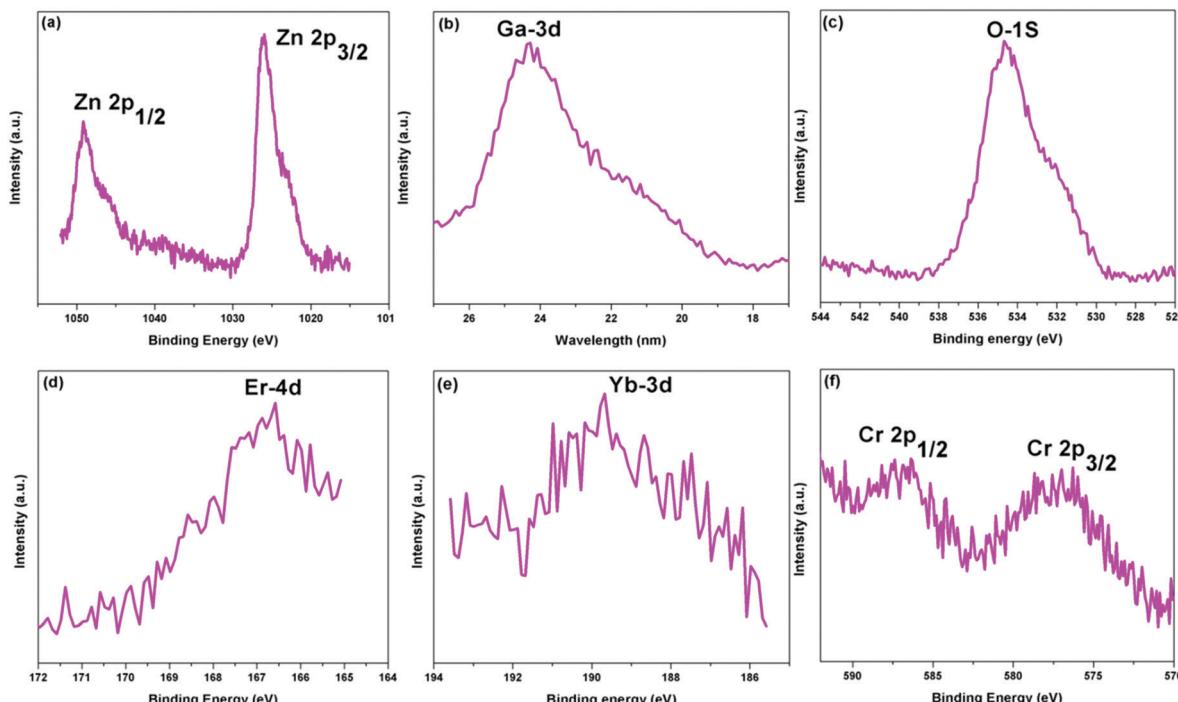

Fig. 2 High-resolution XPS spectra of the (a) Zn 2p, (b) Ga 3d, (c) O 1s, (d) Er 4d, (e) Yb 3d, and (f) Cr 2p orbitals of the ZGO-YEC-AP NPs.
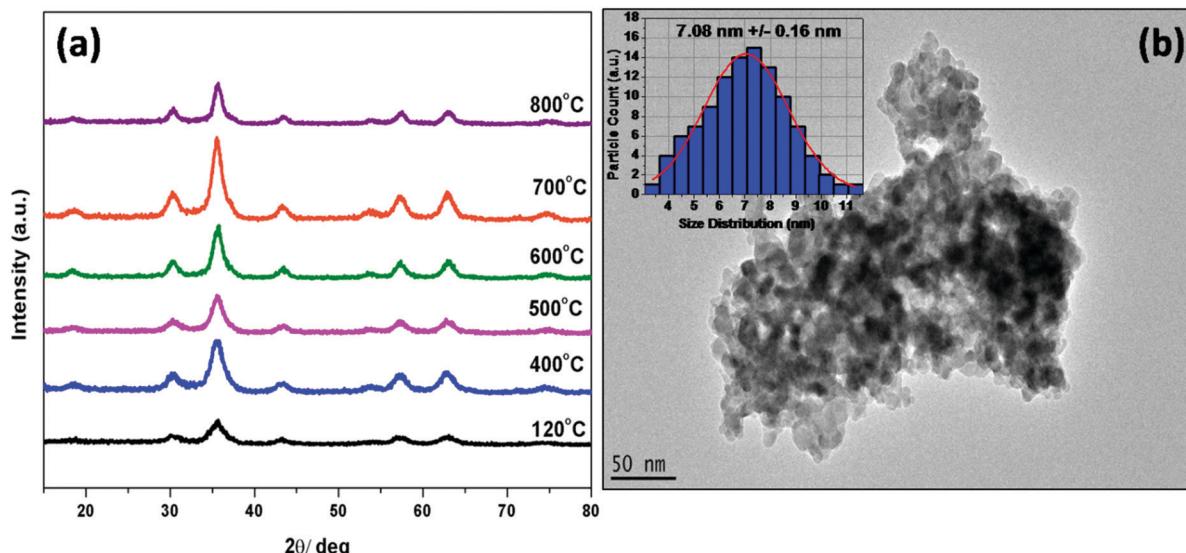
Fig. 3 (a) XRD patterns of the as-prepared ZGO-YEC NPs after annealing at different temperatures. (b) Typical TEM image of the ZGO-YEC-700 NPs.
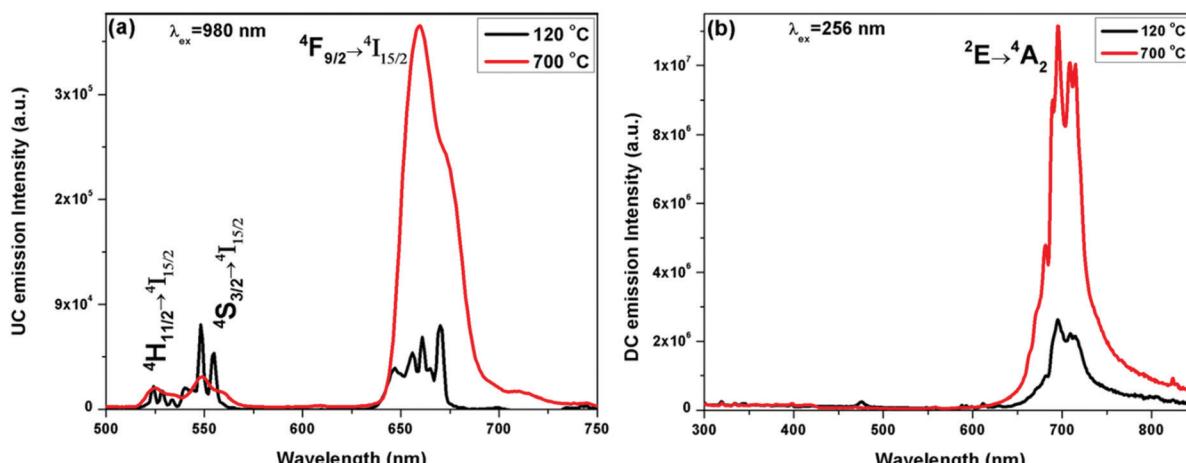

Fig. 4 (a) UC and (b) DC emission spectra of the ZGO-YEC-AP and ZGO-YEC-700 NPs under 980 nm and 254 nm excitation, respectively.

the Cr^{3+} dopant (i) in the unperturbed O_h field and (ii) in the vicinity of defects such as zinc vacancies, zinc interstitials, and antisite defects.[34–36] There are also comprised of Stokes and anti-Stokes phonon bands.[37] Similarly, there was a significant enhancement in the NIR band intensity after thermal treatment of the ZGO-YEC NPs. This increase in the NIR intensity the ZGO-YEC-700 NPs compared to that of the ZGO-YEC-AP NPs is attributed to the substantial decrease in surface defects by thermal annealing at 700 °C. Surface defects are known to provide alterative paths for non-radiative transitions.[38]

These ZGO-YEC NPs are a unique class of luminescence materials, which process three different emissions: (a) DC NIR emission around 700 nm under UV excitation at 254 nm, (b) UC singular red emission (R-band) under 980 nm excitation after annealing at high temperatures, and (c) UC dual red and green emissions under 980 nm excitation from the as-synthesized NPs at 120 °C. This uniqueness is schematically shown in

Fig. S1 (ESI†). Rare earth-doped multicolor light-emitting UC nanophosphors under a single excitation wavelength, e.g. 980 nm in this case, are of high importance in the field of display devices and solid-state lighting. Moreover, the excitation and emission maxima of the ZGO-YCE NPs fall within the "optical window" of tissues. Therefore, they provide both (a) deep percolation of photons upon excitation and (b) large escape depth for the emission in biological samples. Meanwhile, these unique luminescing properties can only be deciphered when the dual excitations and emissions exist simultaneously, which make illegal imitation highly difficult, thereby enhancing and improving the level of anti-counterfeiting.[6]

When the ZGO-YEC-AP and ZGO-YEC-700 NPs were excited by a 980 nm laser under varying powers, no spectral variation was observed. However, monotonic enhancement of the UC emission intensity with an increase in laser power was observed for both the ZGO-YEC-AP and ZGO-YEC-700 NPs (Fig. S3 and S4, respectively,

ESI†). To determine the number of photons involved in the UC process, the following relation was considered:[39]

$$I \propto P^n$$

where I is the integral intensity of a UC luminescence peak, P is the power of the laser, and n is the number of photons involved, which was further elucidated from the slope of the linear plot involving $\log(I)$ vs. $\log(P)$. The logarithmic plots of $\log I$ vs. $\log P$ involving the 550 nm (G-band) and 660 nm (R-band) peaks of the ZGO-YEC-AP NPs and that of only the 660 nm (R′-band) peak of the ZGO-YEC-700 NPs are shown in Fig. S5 (ESI†). From these three plots, it is clearly seen that perfect linearity exists between the UC intensity and laser power. The slopes of these three bands are close to 2.0. This suggests that a two-photon absorption process is involved in the ZGO-YEC-AP NPs for generating green and red emissions as well as in the ZGO-YEC-700 NPs for generating singular red emissions. The correlation coefficient for all these three linear plots was close to 0.99.

The singular red emission requires two different aspects simultaneously: (i) Cr^{3+} co-doping and (ii) critical annealing temperature. Firstly, we discuss the efficacy of Cr^{3+} doping in generating singular red emission in the ZGO-YE NPs. The strong green absorption band of the Cr^{3+} ions eliminates the G-band originating from the up-convertible ZGO-YE NPs. The excitation spectrum of the ZGO:Cr^{3+} NPs under 696 nm emission (Fig. 5a) consists of dual features: (1) a broad band at around 256 nm due to the host excitation band and $O^{2-} \rightarrow Cr^{3+}$ charge transfer band of the ZGO:Cr^{3+} NPs and (2) fine spectral features at around 411 nm (μ_1 = 24 331 cm^{-1}) and 563 nm (μ_2 = 17 762 cm^{-1}), as magnified in the inset of Fig. 6a, which are attributed to $^4A_2 \rightarrow {}^4T_1$ (t^1e^2) and $^4A_2 \rightarrow {}^4T_2$ (t^2e^1) arising from the intra d–d electronic transition of the trivalent Cr^{3+} ions. An intense green band appeared at around 560 nm. As a result, the green photons emitted by the Er^{3+} ions can be efficiently absorbed by Cr^{3+} ions. Furthermore, resonances exist between the Cr^{3+} absorption bands and several metastable Er^{3+} levels in the co-doped ZGO-YEC NPs. As schematically shown in Fig. 5b, the ET process involves energy transfer from the $^2H_{9/2}$
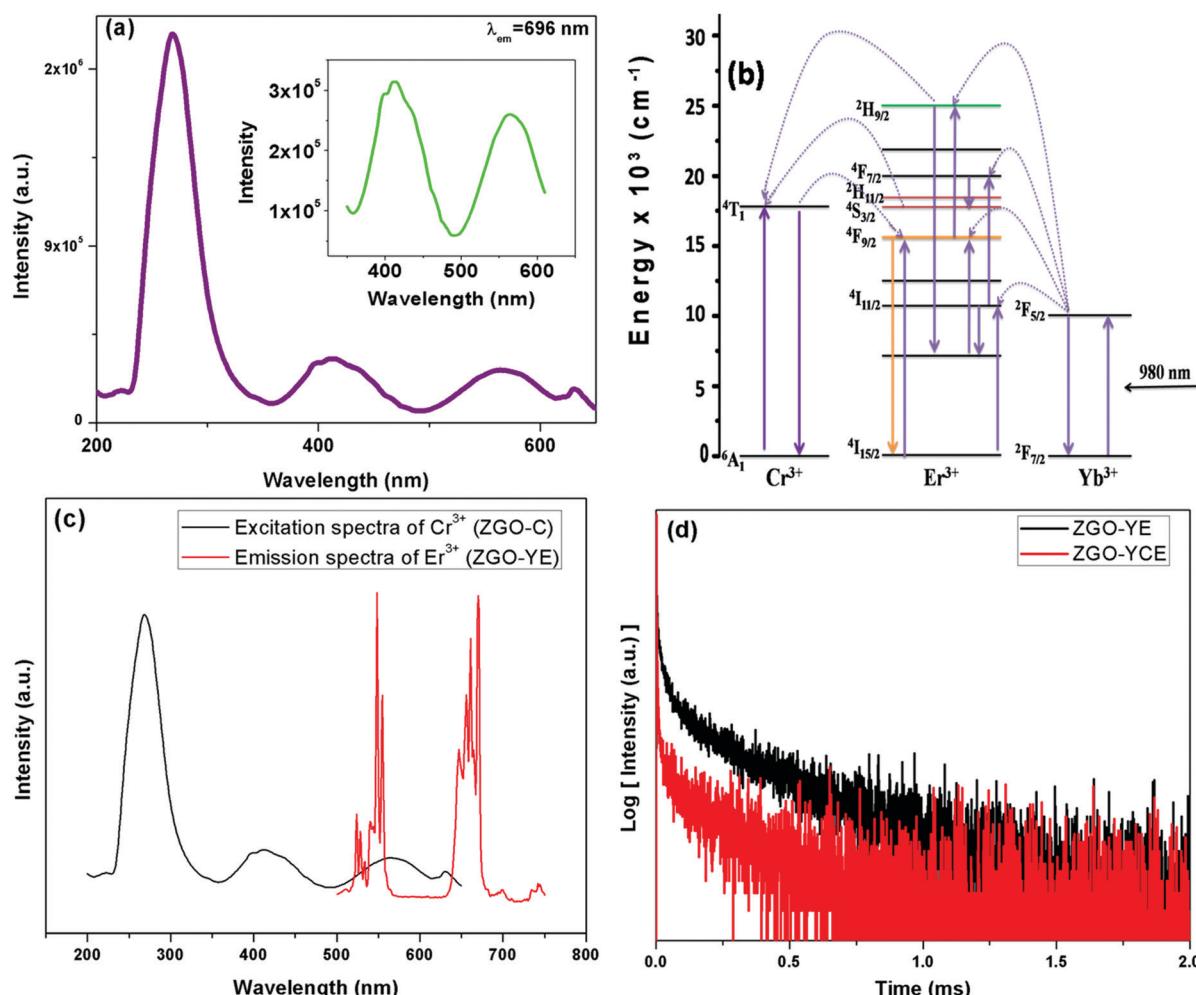
Fig. 5 (a) Excitation spectrum of the ZGO:Cr NPs, (b) proposed mechanism of the ET between dopants of the ZGO-YEC NPs, (c) spectral overlap between the Er^{3+} emission of the ZGO-YE NPs and the Cr^{3+} excitation of the ZGO-C NPs, and (d) decay profiles of Er^{3+} ($^4S_{3/2}$: λ_{em} = 560 nm) of the ZGO-YE and ZGO-YEC NPs.

and $^4S_{3/2}$ levels of the Er^{3+} ions to the $^4T_1$ level of the Cr^{3+} ions followed by back-ET to the $^4F_{9/2}$ level.

The feasibility of ET is validated from Fig. 5c, which clearly shows the spectral overlap between the emissions of Er^{3+} (donor) and the excitation of the Cr^{3+} ion (acceptor). This suggests the high probability of efficient ET between the Er^{3+} and Cr^{3+} ions of the ZGO-YCE NPs.[40,41] To further confirm our explanation for the singular red emission that the green photons emitted from Er^{3+} are efficiently transferred to Cr^{3+}, the luminescence decay profiles

of the ZGO-WE and ZGO-YEC NPs were recorded (Fig. 5d). The reduction in the lifetime of the Er^{3+} green emission from 89 µs to 31 µs upon Cr^{3+} co-doping suggests the efficient ET from the Er^{3+} to the Cr^{3+} ion in the ZGO-YCE NPs. This is then followed by back-ET to Er^{3+}, leading to singular red emission.

3.2.2 Thermal treatment induced singular red emission. To systematically investigate the annealing effects on the ZGO-YEC-AP NPs, they were subjected to thermal treatment in the temperature range of 400–800 °C. Their UC emission spectra
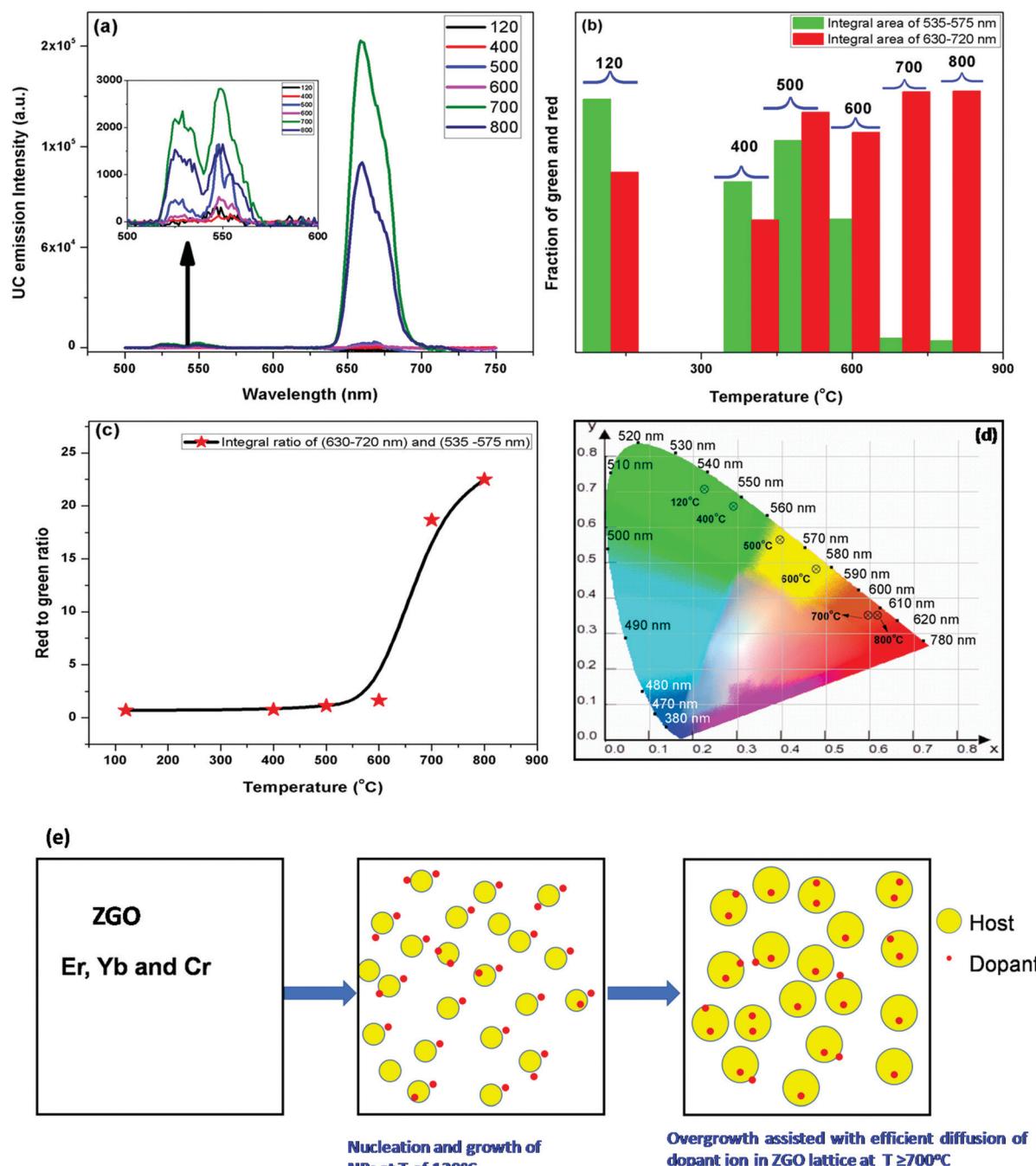

Fig. 6 (a) UC emission spectra, (b) fractional distributions of green- and red-band intensities, (c) R/G band intensity ratio, and (d) color coordinates of the ZGO-YEC NPs after thermal annealing. (e) Schematic showing that post-synthesis annealing is required for the efficient diffusion and even distribution of the Yb^{3+}, Er^{3+}, and Cr^{3+} dopant ions into the ZGO host lattice.

6376 | *J. Mater. Chem. C*, 2020, **8**, 6370–6379

This journal is © The Royal Society of Chemistry 2020

(Fig. 6a) consist both the G- and R-bands after the ZGO-YEC-AP NPs were treated up to 600 °C. Specifically, the ZGO-YEC-AP and ZGO-YEC-400 NPs show a higher G-band intensity compared to that of the R-band (Fig. 6b). Thereafter, the ZGO-YEC-500 and ZGO-YEC-600 NPs start showing dominance of the R-band over the G-band while a fraction of the G-band is still quite high with the R/G ratio close to 1.0 after annealing at 600 °C (Fig. 6c). For the ZGO-YEC-700 and ZGO-YEC-800 NPs, the green band almost completely disappears, except for a single red emission (Fig. 6b and c). Based on the calculated color coordinates, we observed a delightful thermally induced color tunability of the ZGO-YEC NPs (Fig. 6d). More specifically, the ZGO-YEC-AP and ZGO-YEC-400 NPs show green emission, the ZGO-YEC-500 and ZGO-YEC-600 NPs have yellow emission, and the ZGO-YEC-700 and ZGO-YEC-800 NPs process beautiful and bright red emission. The absorption of green emission *via* $Er^{3+} \rightarrow Cr^{3+}$ ET followed by back ET to the $^4F_{9/2}$ level of Er^{3+} depends strongly on the doping effectiveness. When the dopant ions are partially or fully present on particle surface, the energy transfer efficiency (ETE) is inefficient, so there is a substantially intense green emission band together with the red emission band of Er^{3+}. Based on the data shown in Fig. 4a and 6b, c, we believe that the ideal annealing temperature for the effective and complete inclusion of the dopant ions into the host lattice is in the range of 700–800 °C. A plausible schematic of the thermally induced effective diffusion of the dopant ion in the ZGO lattice is shown in Fig. 6e, which clearly shows that high temperature annealing is required for the efficient diffusion and even distribution of the dopant ions into the ZGO host lattice.

To further confirm the fact that a single red emission is achieved *via* the synergistic effect of both Cr^{3+} co-doping and high-temperature annealing and not just through annealing, we carried out emission studies on the as-prepared and 700 °C annealed $ZnGa_2O_4$:Yb^{3+}:Er^{3+} (ZGO-YE, without chromium co-doping) NPs, and their emission spectra are shown in Fig. S2 (ESI†). Accordingly, it can clearly be seen that the PL spectrum of the as-prepared ZGO-YE NPs consists of intense G- and R-bands, the intensity of which increases after annealing at the high temperature of 700 °C. The PL emission enhancement by annealing is attributed to the reduction of surface defects, which are known to provide alternate pathways for non-radiative relaxation.[42]

4. Conclusion

In conclusion, we reported a simple and facile approach for generating a single red emission from $ZnGa_2O_4$:Yb,Er UCNPs through Cr^{3+} co-doping and annealing. The synthesized ultra-fine ZGO-YCE NPs have a strong single red UC emission due to the absorption of green emission *via* $Er^{3+} \rightarrow Cr^{3+}$ ET followed by back ET to the $^4F_{9/2}$ level of Er^{3+}. The red-green ratio (RGR) of around 23 was achieved by annealing the as-synthesized ZGO-YCE NPs at 800 °C. The ZGO-YCE NPs also showed a DC NIR emission at around 700 nm under UV excitation, while the as-prepared ZGO-YCE NPs showed dual red and green UC emission under 980 nm excitation. These multicolor emissions

from a single set of materials by tuning the annealing temperature and excitation wavelength can be beneficial in security applications. The fact that the Cr^{3+} ion is paramagnetic in nature makes the ZGO-YCE NPs potential bio-labels in magnetic resonance imaging. As a result of their highly intense red emission, these UCNPs may be suitable for biological imaging, security applications and display devices.

Conflicts of interest

There are no conflicts to declare.

Acknowledgements

References

1 R. L. Rungta, B.-F. Osmanski, D. Boido, M. Tanter and S. Charpak, Light controls cerebral blood flow in naive animals, *Nat. Commun.*, 2017, **8**, 14191.

2 H. Ye, M. Daoud-El Baba, R.-W. Peng and M. Fussenegger, A synthetic optogenetic transcription device enhances blood-glucose homeostasis in mice, *Science*, 2011, **332**, 1565–1568.

3 Q. Mei, A. Bansal, M. K. G. Jayakumar, Z. Zhang, J. Zhang, H. Huang, D. Yu, C. J. A. Ramachandra, D. J. Hausenloy, T. W. Soong and Y. Zhang, Manipulating energy migration within single lanthanide activator for switchable upconversion emissions towards bidirectional photoactivation, *Nat. Commun.*, 2019, **10**, 4416.

4 S. K. Gupta, M. A. P. Garcia, J. P. Zuniga, M. Abdou and Y. Mao, Visible and ultraviolet upconversion and near infrared downconversion luminescence from lanthanide doped $La_2Zr_2O_7$ nanoparticles, *J. Lumin.*, 2019, **214**, 116591.

5 S. Xue, H. Deng, Q. Xie, Y. Hu, J. Yan, X. Zhao, F. Wang, Q. Zhang, L. Luo, C. Deng, C. He, D. Lin, S. Li, X. A. Wang and H. Luo, Giant tunability of upconversion photoluminescence in Er^{3+}-doped $(K,Na)NbO_3$ single crystals, *Nanoscale*, 2019, **11**, 16928–16934.

6 J. Xu, B. Zhang, L. Jia, Y. Fan, R. Chen, T. Zhu and B. Liu, Dual-Mode, Color-Tunable, Lanthanide-Doped Core–Shell Nanoarchitectures for Anti-Counterfeiting Inks and Latent Fingerprint Recognition, *ACS Appl. Mater. Interfaces*, 2019, **11**, 35294–35304.

7 R. Lv, M. Feng, J. Liu, X. Jiang, H. Yuan, R. Yan and J. Tian, Improved Red Emission and Short-Wavelength Infrared Luminescence under 808 nm Laser for Tumor Theranostics, *ACS Biomater. Sci. Eng.*, 2019, **5**, 4683–4691.

8 Q.-C. Sun, Y. Ding and P. Nagpal, Photophysical Color Tuning for Photon Upconverting Nanoparticles, *ACS Appl. Mater. Interfaces*, 2019, **11**, 27011–27016.

9 M. Li, Z. Yang, Y. Ren, J. Ruan, J. Qiu and Z. Song, Reversible Modulated Upconversion Luminescence of MoO_3:Yb^{3+},Er^{3+} Thermochromic Phosphor for Switching Devices, *Inorg. Chem.*, 2019, **58**, 6950–6958.

10 S. K. Gupta, M. Abdou, J. P. Zuniga, A. Puretzky and Y. Mao, Smarium activated $La_2Hf_2O_7$ nanoparticles as multifunctional phosphors, *ACS Omega*, 2019, **4**(19), 17956–17966.

11 S. K. Gupta, J. P. Zuniga, M. Abdou, M. P. Thomas, M. D. A. Goonatilleke, B. S. Guiton and Y. Mao, Lanthanide-doped lanthanum hafnate nanoparticles as multicolor phosphors for warm white lighting and scintillators, *Chem. Eng. J.*, 2020, **379**, 122314.

12 D. Przybylska, A. Ekner-Grzyb, B. F. Grześkowiak and T. Grzyb, Upconverting SrF_2 nanoparticles doped with Yb^{3+}/Ho^{3+}, Yb^{3+}/Er^{3+} and Yb^{3+}/Tm^{3+} ions – optimisation of synthesis method, structural, spectroscopic and cytotoxicity studies, *Sci. Rep.*, 2019, **9**, 8669.

13 B. B. Srivastava, A. Kuang and Y. Mao, Persistent luminescent sub-10 nm Cr doped $ZnGa_2O_4$ nanoparticles by a biphasic synthesis route, *Chem. Commun.*, 2015, **51**, 7372–7375.

14 Z. Bai, H. Lin, J. Johnson, S. C. Rong Gui, K. Imakita, R. Montazami, M. Fujii and N. Hashemi, The single-band red upconversion luminescence from morphology and size controllable Er^{3+}/Yb^{3+} doped MnF_2 nanostructures, *J. Mater. Chem. C*, 2014, **2**, 1736–1741.

15 G. Tian, Z. Gu, L. Zhou, W. Yin, X. Liu, L. Yan, S. Jin, W. Ren, G. Xing, S. Li and Y. Zhao, Mn^{2+} Dopant-Controlled Synthesis of $NaYF_4$:Yb/Er Upconversion Nanoparticles for in vivo Imaging and Drug Delivery, *Adv. Mater.*, 2012, **24**, 1226–1231.

16 X. Gao, D. Xu, J. Du, J. Li, Z. Yang and J. Sun, Tunability of green–red up-conversion emission of co-doped Ca_3WO_6:Yb^{3+}/Er^{3+} powders, *J. Mater. Sci.: Mater. Electron.*, 2017, **28**, 16540–16546.

17 D. Xu, C. Liu, J. Yan, S. Yang and Y. Zhang, Understanding energy transfer mechanisms for tunable emission of Yb^{3+}–Er^{3+} codoped GdF_3 nanoparticles: concentration-dependent luminescence by near-infrared and violet excitation, *J. Mater. Chem. C*, 2015, **119**, 6852–6860.

18 Y. Zhang, J. Liu, Y. Ji, D. Li, J. Xu, L. Xu and K. Chen, Enhanced up-conversion red light emission from rare earth titanium oxide nanocrystals with pyrochlore phase, *Opt. Mater. Express*, 2018, **8**, 2643–2653.

19 M.-Y. Xie, X.-N. Peng, X.-F. Fu, J.-J. Zhang, G.-L. Li and X.-F. Yu, Synthesis of Yb^{3+}/Er^{3+} co-doped MnF_2 nanocrystals with bright red up-converted fluorescence, *Scr. Mater.*, 2009, **60**, 190–193.

20 Z. Bai, H. Lin, J. Johnson, S. C. R. Gui, K. Imakita, R. Montazami, M. Fujii and N. Hashemi, The single-band red upconversion luminescence from morphology and size controllable Er^{3+}/Yb^{3+} doped MnF_2 nanostructures, *J. Mater. Chem. C*, 2014, **2**, 1736–1741.

21 Z. Bai, H. Lin, K. Imakita, R. Montazami, M. Fujii and N. Hashemi, Synthesis of Er^{3+}/Yb^{3+} codoped $NaMnF_3$ nanocubes with single-band red upconversion luminescence, *RSC Adv.*, 2014, **4**, 61891–61897.

22 J. Wang, F. Wang, C. Wang, Z. Liu and X. Liu, Single-Band Upconversion Emission in Lanthanide-Doped $KMnF_3$ Nanocrystals, *Angew. Chem., Int. Ed.*, 2011, **50**, 10369–10372.

23 H. Lin, D. Xu, A. Li, Z. Qiu, S. Yang and Y. Zhang, Enhanced red upconversion emission and its mechanism in Yb^{3+}–Er^{3+} codoped α-$NaLuF_4$ nanoparticles, *New J. Chem.*, 2017, **41**, 1193–1201.

24 M. Tuomisto, E. Palo, T. Laihinen, I. Hyppänen, M. Lastusaari, H. C. Swart and J. Hölsä, Effect of Mn and Cr doping on the up-conversion luminescence from $NaYF_4$:Yb^{3+},Er^{3+}, *Opt. Mater.*, 2016, **59**, 115–119.

25 I. Mikalauskaite, G. Pleckaityte, M. Skapas, A. Zarkov, A. Katelnikovas and A. Beganskiene, Emission spectra tuning of upconverting $NaGdF_4$:20% Yb, 2% Er nanoparticles by Cr^{3+} co-doping for optical temperature sensing, *J. Lumin.*, 2019, **213**, 210–217.

26 S. Ye, E. Song, E. Ma, S. Zhang, J. Wang, X. Chen, Q. Zhang and J. Qiu, Broadband Cr^{3+}-sensitized upconversion luminescence in $La_3Ga_5GeO_{14}$:Cr^{3+},Yb^{3+},Er^{3+}, *Opt. Mater. Express*, 2014, **4**, 638–648.

27 B. T. Huy, Z. Gerelkhuu, J. W. Chung, V.-D. Dao, G. Ajithkumar and Y.-I. Lee, Enhanced light harvesting with chromium in $NaLu_{0.70-x}Gd_{0.10}F_4$:$Yb_{0.18}Er_{0.02}Cr_x$ $(0 \leq x \leq 0.25)$ upconversion system, *Mater. Sci. Eng., B*, 2017, **223**, 91–97.

28 F.-F. Chen, Z.-Q. Chen, Z.-Q. Bian and C.-H. Huang, Sensitized luminescence from lanthanides in d–f bimetallic complexes, *Coord. Chem. Rev.*, 2010, **254**, 991–1010.

29 L. Aboshyan-Sorgho, M. Cantuel, S. Petoud, A. Hauser and C. Piguet, Optical sensitization and upconversion in discrete polynuclear chromium–lanthanide complexes, *Coord. Chem. Rev.*, 2012, **256**, 1644–1663.

30 Y. Cheng, K. Sun, P. Ge and R. Liu, Color-tunable up-conversion luminescence of $Zn(Al_xGa_{1-x})_2O_4$:Yb^{3+},Tm^{3+},Er^{3+} powders, *Ceram. Int.*, 2018, **44**, 18090–18097.

31 Y. Cheng, K. Sun and P. Ge, Up-conversion luminescence in Yb^{3+}/Er^{3+} co-doped $ZnGa_2O_4$ and $ZnAl_2O_4$ powder phosphors, *Optik*, 2018, **170**, 1–9.

32 Z. Li, Y. Zhang, X. Wu, L. Huang, D. Li, W. Fan and G. Han, Direct Aqueous-Phase Synthesis of Sub-10 nm "Luminous Pearls" with Enhanced in Vivo Renewable Near-Infrared Persistent Luminescence, *J. Am. Chem. Soc.*, 2015, **137**, 5304–5307.

33 Y. Liu, Y. Lu, X. Yang, X. Zheng, S. Wen, F. Wang, X. Vidal, J. Zhao, D. Liu, Z. Zhou, C. Ma, J. Zhou, J. A. Piper, P. Xi and D. Jin, Amplified stimulated emission in upconversion nanoparticles for super-resolution nanoscopy, *Nature*, 2017, **543**, 229.

34 N. Basavaraju, K. R. Priolkar, D. Gourier, S. K. Sharma, A. Bessière and B. Viana, The importance of inversion disorder in the visible light induced persistent luminescence in Cr^{3+} doped AB_2O_4 (A = Zn or Mg and B = Ga or Al), *Phys. Chem. Chem. Phys.*, 2015, **17**, 1790–1799.

35 W. Nie, F. Michel-Calendini, C. Linares, G. Boulon and C. Daul, New results on optical properties and term-energy calculations in Cr^{3+}-doped $ZnAl_2O_4$, *J. Lumin.*, 1990, **46**, 177–190.

36 W. Zhang, J. Zhang, Z. Chen, T. Wang and S. Zheng, Spectrum designation and effect of Al substitution on the luminescence of Cr^{3+} doped $ZnGa_2O_4$ nano-sized phosphors, *J. Lumin.*, 2010, **130**, 1738–1743.

37 A. l. Bessière, S. K. Sharma, N. Basavaraju, K. R. Priolkar, L. Binet, B. Viana, A. J. Bos, T. Maldiney, C. Richard and D. Scherman, Storage of visible light for long-lasting phosphorescence in chromium-doped zinc gallate, *Chem. Mater.*, 2014, **26**, 1365–1373.

38 S. K. Gupta, J. P. Zuniga, M. Abdou and Y. Mao, Thermal annealing effects on $La_2Hf_2O_7:Eu^{3+}$ nanoparticles: a curious case study of structural evolution and site-specific photo-and radio-luminescence, *Inorg. Chem. Front.*, 2018, **5**, 2508–2521.

39 F. Vetrone, J.-C. Boyer, J. A. Capobianco, A. Speghini and M. Bettinelli, Significance of Yb^{3+} concentration on the upconversion mechanisms in codoped $Y_2O_3:Er^{3+},Yb^{3+}$ nanocrystals, *J. Appl. Phys.*, 2004, **96**, 661–667.

40 S. K. Gupta, P. S. Ghosh, N. Pathak, A. Arya and V. Natarajan, Understanding the local environment of Sm^{3+} in doped $SrZrO_3$ and energy transfer mechanism using time-resolved luminescence: a combined theoretical and experimental approach, *RSC Adv.*, 2014, **4**, 29202–29215.

41 S. K. Gupta, M. Abdou, J. P. Zuniga, A. A. Puretzky and Y. Mao, Samarium-Activated $La_2Hf_2O_7$ Nanoparticles as Multifunctional Phosphors, *ACS Omega*, 2019, **4**, 17956–17966.

42 S. K. Gupta, K. Sudarshan, P. S. Ghosh, A. P. Srivastava, S. Bevara, P. K. Pujari and R. M. Kadam, Role of various defects in the photoluminescence characteristics of nanocrystalline $Nd_2Zr_2O_7$: an investigation through spectroscopic and DFT calculations, *J. Mater. Chem. C*, 2016, **4**, 4988–5000.

This journal is © The Royal Society of Chemistry 2020

J. Mater. Chem. C, 2020, **8**, 6370–6379 | **6379**